Research Article | Vol. 31, No. 21 / 9 Oct 2023 / Optics Express 35387

Optics EXPRESS

Curvature dependent onset of quantum tunneling in subnanometer gaps

MANDANA JALALI,[1] JAN TARO SVEJDA,[1] JESIL JOSE,[2] SEBASTIAN SCHLÜCKER,[2] AND DANIEL ERNI[1,*]

[1] *General and Theoretical Electrical Engineering (ATE), Faculty of Engineering, University of Duisburg-Essen, and CENIDE – Center for Nanointegration Duisburg-Essen, 47048 Duisburg, Germany*
[2] *Chair of Physical Chemistry I, Department of Chemistry, University of Duisburg-Essen, and CENIDE – Center for Nanointegration Duisburg-Essen, Universitätsstr. 5, 45141 Essen, Germany*
[*] *daniel.erni@uni-due.de*

Abstract: The quantum tunneling in subnanometer gap sizes in gold dimers is studied in order to account for the dependency of the onset of quantum tunneling on the dimer's radius and accordingly the gap wall's curvature, realized in experiments. Several nanodimers both nanowires and nanospheres with various radii and gap sizes are modelled and simulated based on the quantum corrected model, determining the onset of the quantum tunneling. Results show that the onset of quantum tunneling is both dependent on the gap size as well as on the dimer's radius. As larger dimers result in larger effective conductivity volumes, the influence of the quantum tunneling begins in larger gap sizes in larger dimers.

1. Introduction

Plasmonic nanodimers due to their strong field localizations within the gap at their corresponding bonding dimer plasmon (BDP), have been implemented in various applications [1–3]. However, it has been shown that when the gap size, the minimum distance between the two particles, is about 1 nm or even smaller, quantum tunneling (QT) can occur, which reduces the expected field localization within the gap predicted by classical electrodynamics [4]. Hence, while reducing the gap size the expected redshift in the BDP is transformed into a blueshift due to the QT presence [5]. Highly uniform gold nanosphere dimers [6] with 15, 25, 40 nm radii are fabricated, where the gap sizes are precisely controlled by corresponding alkane dithiol linker molecules with varying number of carbon atoms in the chain, providing a subnanometer control (with an inaccuracy lower than 0.05 nm in all the cases) over the gap distances. Such precise fabrication techniques further allowed for determining the spectral position of the BDP in all the mentioned dimers, which revealed that such QT not only depends on the gap size but also the particle's curvature confining the gap [7]. Results show that the quantum regime and correspondingly the QT starts at larger gap sizes in larger dimers. In this study, and in order to provide insights about the underlying mechanisms for the observed curvature dependence onset of QT in subnanometer gaps, based on a classical effective model namely the Quantum Corrected Model (QCM) [8], the gold dimers are modelled and simulated, with the objective of scrutinizing the gap's shape and size effect on the onset of quantum tunneling within the mentioned dimers and accordingly providing insights for the observed size-dependent onset of quantum tunneling in gold dimers.

2. Accurate modelling of a subnanometer gap

Since the gap sizes are in the range of only few nanometers, nonlocality has to be taken into account, as the electron scattering from the particle's boundaries effect the mean free path of the conducting electrons [9,10]. The nonlocality is incorporated according to the hydrodynamic model (HM) [11–14]. In this approach, the nonlocal material properties of the nanodimers are

#500611 https://doi.org/10.1364/OE.500611
Journal © 2023 Received 24 Jul 2023; revised 10 Sep 2023; accepted 26 Sep 2023; published 6 Oct 2023

Optics EXPRESS

described based on the nonlocal phasor polarization current $\mathbf{J}_{\mathrm{hd}}$, which is coupled to the electric field $\mathbf{E}$ through the following equations [15,16].

$$[\nabla \times \nabla \times -\varepsilon_1(\omega)\frac{\omega^2}{c^2}]\mathbf{E}(\mathbf{r},\omega) = i\omega\mu_0\mathbf{J}_{\mathrm{hd}}(\mathbf{r},\omega) \tag{1}$$

$$[\nabla^2 + \frac{\omega(\omega+i\gamma)}{\beta^2}]\mathbf{J}_{\mathrm{hd}}(\mathbf{r},\omega) = \frac{i\varepsilon_0\omega_{\mathrm{P}}\omega}{\beta^2}\mathbf{E}(\mathbf{r},\omega) \tag{2}$$

In which ω is the angular frequency, $\gamma = 1/\tau$, where τ is the relaxation time of the free electron gas, ω_{P} is the plasma frequency of gold, while the dimension dependent nonlocal-response parameter $\beta = \sqrt{\frac{3}{4}}v_F$ is related to the Fermi velocity.

To account for the QT probability instead of a full quantum mechanical approach such as, e.g., an elaborate time-domain density functional theory-based analysis (TD-DFT) [17], which for such big structures is not tractable, the quantum corrected model (QCM) is introduced [5]. In the QCM, the QT is translated into artificial conductivity of the gap and then is accounted for via defining a fictitious material for the gap [8,18]. This artificial conductivity is dependent on the nanowires separation distance l at each height, and consequently on the nanowires curvature (cf.Figure 1(a))). The aforementioned artificial conductivity is determined based on the following fictitious Drude permittivity along with the corresponding conductivity:

$$\varepsilon_{\mathrm{g}}(\omega,l) = \varepsilon_0(\omega) + (\varepsilon_{\mathrm{m}}^{\mathrm{d}}(\omega) - \varepsilon_0(\omega))\exp\frac{-l}{l_{\mathrm{d}}} - \frac{\omega_{\mathrm{P}}^2}{\omega(\omega+i\gamma_g(l))} \tag{3}$$

$$\sigma_g(\omega,l) = -i\omega\varepsilon_0[\varepsilon_g(\omega,l) - 1] \tag{4}$$

In which the $\gamma_{\mathrm{g}}(l) = \gamma_{\mathrm{P}}\exp\frac{-l}{l_{\mathrm{c}}}$ is the l dependent loss parameter with the phenomenological decay length of $l_{\mathrm{c}} = 0.4$Å. In the cases of noble metals such gold, d-electrons, which are the electrons in d-subshell in the corresponding electronic structure of the noble metal, play a vital role in their optical response, and accordingly their contribution should be taken into account [8]. The second term in the Eq. (3) accounts for the contribution of such d-electrons to the optical response of the dimer, in which the dispersive $\varepsilon_{\mathrm{m}}^{\mathrm{d}}$ associates the interband transitions involving d-electrons with the decay length of $l_{\mathrm{d}} = 0.8$Å and, hence, to the resulting conductivity. The values for $l_{\mathrm{c}}, l_{\mathrm{d}}$ are taken from [8], where the l_{c} is determined while comparing the QCM with the full quantum mechanical TD-DFT results in case of small nanoparticles, where such comparison is feasible, and the l_{d} is taken from the radial decay of the 5d orbital. These values are fixed for all dimers and gap sizes.

The schematic of the simulation domain is depicted in the Fig. 1(a)). The simulation model is based on classical electrodynamics in the finite element method (FEM) based COMSOL Multiphysics software and the simulations are carried out in three different frameworks. The first framework is a classical model (CM) based on Maxwell equations, while in the second framework, the nonlocal model (NM), the effect of nonlocality based on the HM is considered. This has been implemented within the software via adding the Eq. (2) as a partial differential equation (PDE) for the nanowires and the gap, while the nonlocal phasor polarization current vanishes at the nanowires surface but is continuous at the nanodimer gap boundary. The mentioned equation is additionally coupled to the Maxwell equation (Eq. (1)). Finally, the third framework provides a full picture of all underlying mechanisms comprising of both nonlocality as well as the QT probability, where the former is based on the HM and the latter based on the QCM. This framework, here referred to as the QCM, is incorporated within the software through defining the fictitious Drude permittivity for the gap, in a model where nonlocality is already included.

Optics EXPRESS

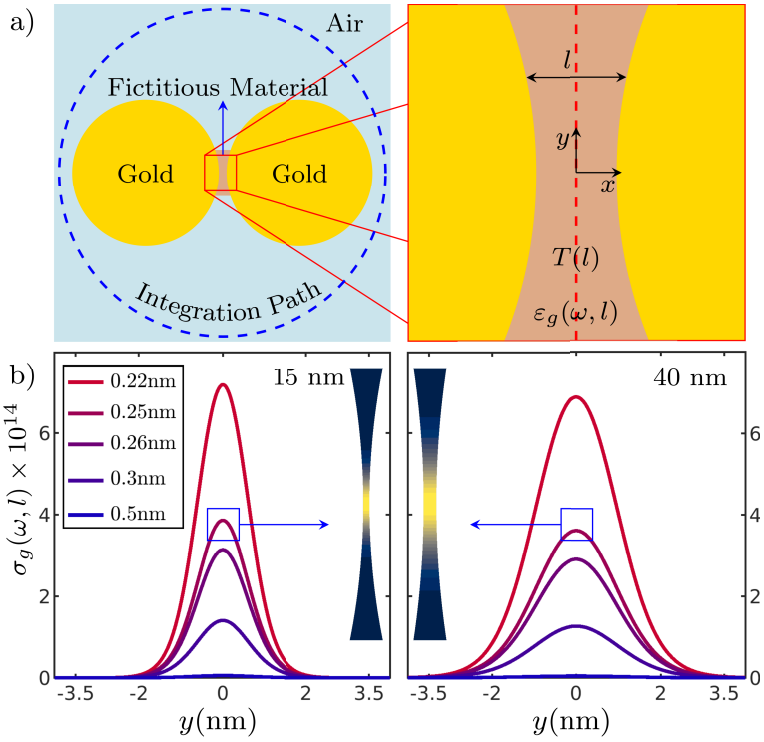

Fig. 1. a) The schematic of the simulation domain where a fictitious conductive material distribution is defined within the gap region which takes into account the quantum tunneling probability. b) The corresponding fictitious conductivity distribution along the $y-$axis within the gap (red dashed line) for various gap sizes in 15 nm and 40 nm dimers. The inset shows the corresponding conductivity distributions for a gap size of 0.25 nm.

3. Results and discussion

The conductivity (cf. Eq. (3)) in the cases of 15 nm and 40 nm for various gap sizes are illustrated in the Fig. 1(b)), which shows that although the conductivity's maximum is only dependent on the minimum separation of the walls, the spatial distribution of the conductivity is determined by the dimer's radius and gets larger for larger radii. This results in a particle's surface curvature-dependent conductivity distribution as depicted in the inset of the Fig. 1(b)). Gold nanowires with various radii (namely 10 nm, 15 nm, 25 nm, 30 nm, and 40 nm) and subnanometer gap sizes ranging from 0.1nm up to 2nm are simulated in the frameworks of the CM, the NM, as well as the QCM. Through integrating the poynting vector over the integration path (cf. Figure 1(a))), the normalized extinction cross section is calculated which determines the spectral position of charge transfer plasmon (CTP) and the BDP. It should be mentioned here, that the QT in the case of CTP is direct charge transfer QT due to small size of the gap, and also the observed QT in the BDP are result of direct charge transfer as the nonlocal screening through modifying the classical border of the nanoparticles surface, reduces the potential barrier amongst the two metallic surfaces and accordingly facilitate quantum tunneling within the gap [19–23]. The resulted quantum tunneling currents are presented in the Visualization 1.

The normalized extinction cross sections, in the QCM framework, for 15 nm and 40 nm dimers are depicted in the Fig. 2 for gap sizes ranging from 0.1 nm up to 2 nm, where the spectral positions of CTPs and BDPs are indicated via red and black arrows respectively. As the CTP

Optics EXPRESS

occurs only in very small gap sizes, such mode is only observed in the case of 0.1 nm gap size, while the BDP occurs in all gap sizes with varying spectral positions. Reducing the gap size introduces the classically predicted redshift in the BDP, however at the 0.26 nm gap the trend modifies into a blueshift which indicates the presence of QT within the gap. It's worth mentioning that in smaller dimers (namely with 10 nm and 15 nm particle sizes), in the case of the 0.24 nm gap size, where the QT is prevailing, spectral position of the BDP seems to be better represented by the turning point instead of the peak in the spectral response of the normalized extinction cross sections (cf. the blue arrow within the Fig. 2), and hence is indicated with a blue arrow.

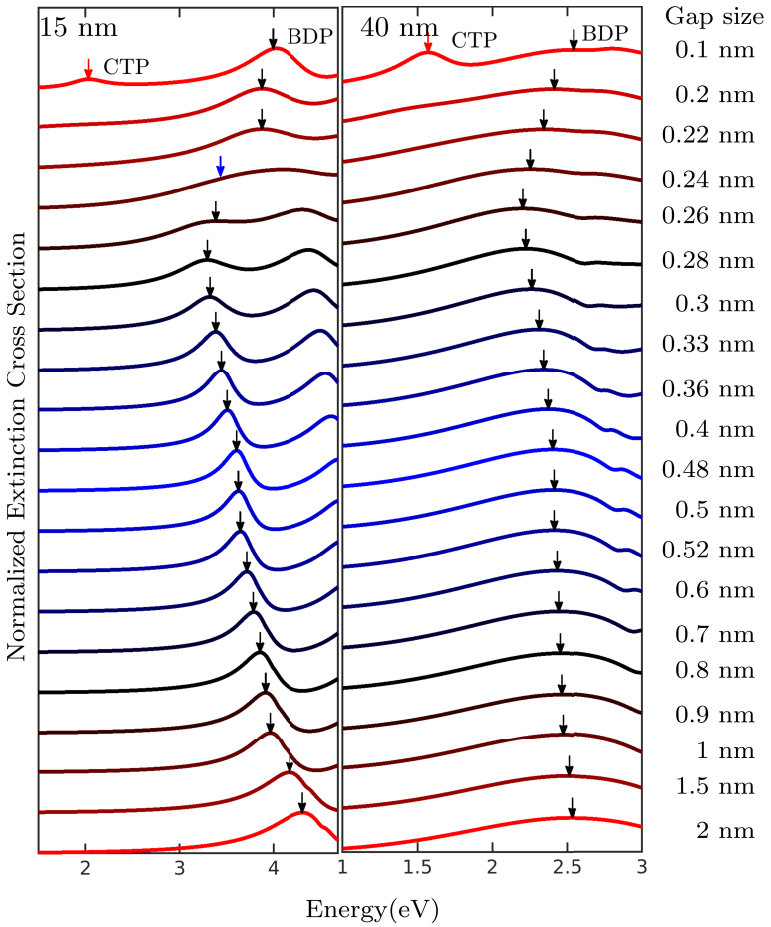

Fig. 2. The spectral response of the normalized extinction cross sections, in the QCM framework, for 15 nm (left) and 40 nm (right) dimers for various gap sizes, where the red arrows show the charge transfer plasmon modes (CTP), while the black arrows show the bonding dimer plasmon modes (BDP).

The spectral position of the BDPs at each gap size for 15 nm and 40 nm dimers in all the three frameworks are depicted in the Fig. 3. It can be seen that for the 40 nm dimer in large gap sizes the classical model is in accordance with the NM and QCM, which indicates a classical regime (yellow highlighted region). Decreasing the gap size, the NM and QCM starts to deviate from the classical prediction, however both are virtually identical, which demonstrate a nonlocal regime (red highlighted region), in which nonlocality plays a role however no quantum tunneling effect is evident. In smaller gaps namely at 0.52 nm in the case of 40 nm dimer, the QCM starts to

Optics EXPRESS

deviate from the NM implying the onset of QT and correspondingly the quantum regime (blue highlighted region). In the case of the 15 nm dimer, even for the 2 nm gap size, the classical model fails to predict the correct results, as due to the small size of nanowires, nonlocality already has to be taken into account. In this case, at the 0.48 nm gap size, the QCM deviates from the NM, marking the onset of the quantum regime. Further reducing the gap size, the quantum tunneling current becomes prevailing which leads to a blueshift in BDP spectral position at the 0.26 nm gap in all dimers.

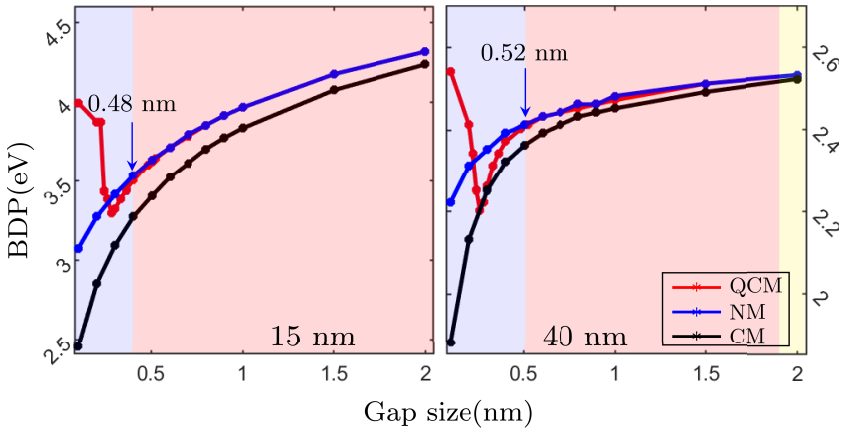

Fig. 3. The bonding dimer plasmon (BDP) modes versus the gap size in 15 nm (left), and 40 nm (right) dimers based on the quantum corrected model (QCM), the nonlocal model (NM), and the classical model (CM).

The spectral position of BDPs for each gap sizes is fitted to a non-uniform fitting function given by the following expression.

$$f(x) = \frac{1}{\Gamma(\kappa)\theta^{\kappa}} x^{\kappa-1} e^{\frac{x}{\theta}} \tag{5}$$

In which $\Gamma(\kappa)$ is the gamma function and θ, κ are the fitting parameters. The derived curves which are fitted to the left and right hand side of the valley (at gap sizes around 0.26 nm) separately, are guides to the eye revealing the trend in which BDPs shift. The curves accompanied by the BDPs as markers are illustrated in the Fig. 4 for all dimers. It is seen that the valley slope is smaller for larger dimers, as the onset of quantum regime occurs in larger gap sizes confirming the dependency of QT on the particle's surface curvature as observed in the corresponding experiments, where the onset of quantum tunnelling occurs at 0.96 ± 0.04nm gap size for the case of 40 nm radius dimer, at 0.83 ± 0.03nm for the case of 25 nm radius dimer, and at 0.72 ± 0.02nm for the case of 15 nm radius dimer [6,7].

To determine the gap's readiness in allowing both the hydrodynamic and the quantum tunneling current to cross, a new parameter namely the hydrodynamic conductivity of the gap per unit area is defined based on the following relation:

$$\sigma_{\text{qhd}} = \frac{\int_{\text{gap}} \frac{|\mathbf{J}_{\text{qhd}}|}{|\mathbf{E}|} dV}{(1\text{m}^2)} \tag{6}$$

In which $\mathbf{J}_{\text{qhd}}$ is the hydrodynamic current which incorporates also the quantum tunneling probability. Such quantum hydrodynamic conductivity per unit area is calculated for each gap size in all considered dimers and the results for gap sizes around the onset of QT, namely 0.26

Optics EXPRESS

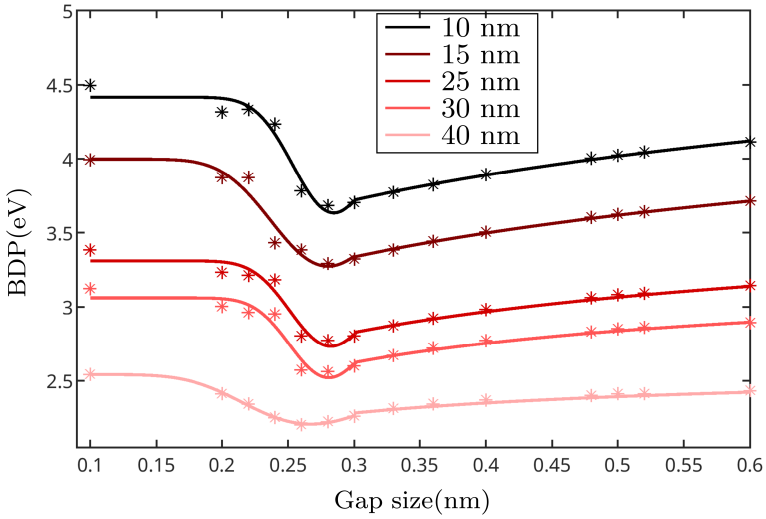

Fig. 4. The bonding dimer plasmon (BDP) modes for various gap sizes in 10 nm, 15 nm, 25 nm, 30 nm, and 40 nm dimers fitted to a non-uniform Gamma fitting function on the left and right side of the valley.

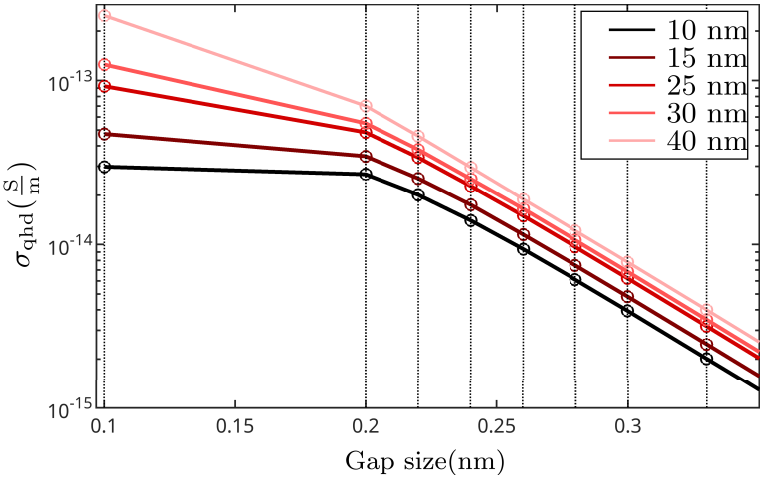

Fig. 5. The quantum hydrodynamic conductivity versus the gap size in 10 nm, 15 nm, 25 nm, 30 nm, and 40 nm dimers. (Visualization 1)

nm, are depicted in the Fig. 5 , which shows that for each gap size, the gap's hydrodynamic conductivity is larger in larger dimers. The gap's quantum hydrodynamic conductivity in the case of the 40 nm dimer not only is larger at each gap size compared to the smaller dimers, but also deviates earlier, which describes the earlier onset of the quantum tunneling in this larger dimer, which is in agreement with the experiments. This is visualized through illustrating the quantum hydrodynamic current $\mathbf{J}_{qhd}$ in both 10 nm and 40 nm dimers while decreasing the gap size at each corresponding BDP modes (see Visualization 1), which demonstrates how the hydrodynamic current changes with reducing the gap size. As mentioned, although gold nanowires show the same behavior in terms of nonlocality and QT probability in comparison to spherical dimers, smaller gap volume together with reduced electric field strength in the gap effect the onset of the

Optics EXPRESS

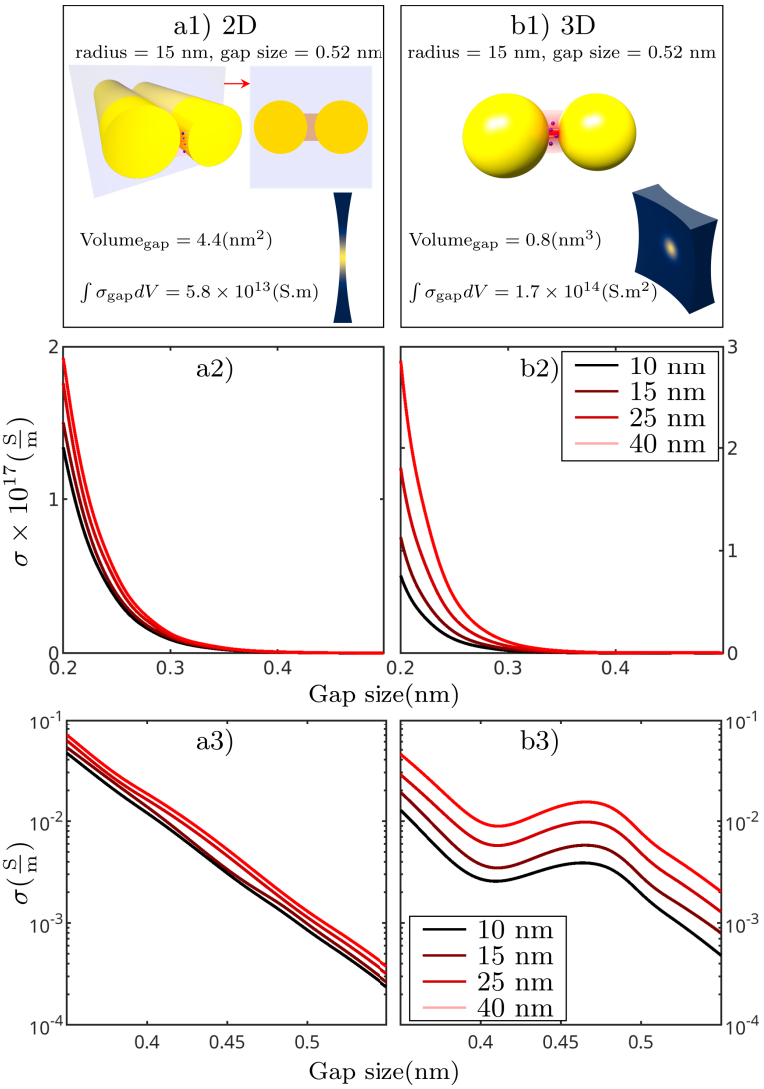

Fig. 6. Artificial conductivity of the gap in a) 2D and b) 3D models. a2 - b2) show the integrated artificial conductivity of the gap versus gap sizes for 10 nm, 15 nm, 25 nm, and 40 nm dimers, and a3 - b3) depict the logarithm of the corresponding integrated artificial conductivity of the gap versus gap sizes for larger gap sizes, namely from 0.35 up to 0.6 nm, which highlights the difference among conductivities in nanowires versus the nanospheres.

QT. The impact of this effect is investigated through modelling gold nanospheres with same radii and gap sizes, in which instead of a full wave simulation, only the artificial conductivities of the gaps are calculated. The results together with the models geometries are presented in the Fig. 6. As expected the integrated artificial conductivity of the gap in spherical dimers is larger compared to the nanowires and also has a stronger dependence of the dimer's particle radius. The stronger dependence of the integrated artificial conductivity of the gap to the dimers radius can be deduced from the larger differences among the integrated artificial conductivity curves for each given radii in the Fig. 6(a2) and (b2). Conclusively the onset of QT in spherical dimers will

Optics EXPRESS

happen already at larger gap sizes and also show stronger dependence of the dimer's particle radius, which result in a radius dependent onset of the QT.

4. Conclusions

In conclusion, we have shown that the quantum tunneling within the subnanomater gap of plasmonic dimers aside from being dependent on the gap size, is also dependent on the dimer's radius and correspondingly the particle's surface curvatures confining the gap region. As dimers with larger radii have reduced wall curvature, they result in a larger effective quantum hydrodynamic conductivity volume and correspondingly in an earlier onset of the quantum tunneling with higher quantum tunneling currents. Based on our results, we deduce that the onset of the blueshift respective to the quantum tunneling in spherical dimers, which for gold nanowire dimers is around 0.26 nm and virtually independent of the dimer's radius, will also be radius/curvature dependent as the effective hydrodynamic conductivity volume and correspondingly the integrated conductivity of the gap are several times larger as already shown in the Fig. 6.

Funding. Deutsche Forschungsgemeinschaft (494809387).

Acknowledgment. We acknowledge support by the Open Access Publication Fund of the University of Duisburg-Essen.

Disclosures. The authors declare no conflicts of interest.

Data availability. Data underlying the results presented in this paper are not publicly available at this time but may be obtained from the authors upon reasonable request.

References

1. E. Prodan and P. Nordlander, "Plasmon hybridization in spherical nanoparticles," J. Chem. Phys. **120**(11), 5444–5454 (2004).
2. H. Aouani, M. Rahmani, and M. Navarro-Cía, *et al.*, "Third-harmonic-upconversion enhancement from a single semiconductor nanoparticle coupled to a plasmonic antenna," Nat. Nanotechnol. **9**(4), 290–294 (2014).
3. K. Höflich, M. Becker, and G. Leuchs, *et al.*, "Plasmonic dimer antennas for surface enhanced raman scattering," Nanotechnology **23**(18), 185303 (2012).
4. J. Zuloaga, E. Prodan, and P. Nordlander, "Quantum description of the plasmon resonances of a nanoparticle dimer," Nano Lett. **9**(2), 887–891 (2009).
5. T. V. Teperik, P. Nordlander, and J. Aizpurua, *et al.*, "Quantum effects and nonlocality in strongly coupled plasmonic nanowire dimers," Opt. Express **21**(22), 27306–27325 (2013).
6. J. H. Yoon, F. Selbach, and L. Schumacher, *et al.*, "Surface plasmon coupling in dimers of gold nanoparticles: Experiment and theory for ideal (spherical) and nonideal (faceted) building blocks," ACS Photonics **6**(3), 642–648 (2019).
7. J. Jose, L. Schumacher, and M. Jalali, *et al.*, "Particle size-dependent onset of the tunneling regime in ideal dimers of gold nanospheres," ACS Nano **16**(12), 21377–21387 (2022).
8. R. Esteban, A. Zugarramurdi, and P. Zhang, *et al.*, "A classical treatment of optical tunneling in plasmonic gaps: extending the quantum corrected model to practical situations," Faraday Discuss. **178**, 151–183 (2015).
9. M. S. Tame, K. McEnery, and Ş. Özdemir, *et al.*, "Quantum plasmonics," Nat. Phys. **9**(6), 329–340 (2013).
10. P. Törmä and W. L. Barnes, "Strong coupling between surface plasmon polaritons and emitters: a review," Rep. Prog. Phys. **78**(1), 013901 (2014).
11. S. Raza, S. I. Bozhevolnyi, and M. Wubs, *et al.*, "Nonlocal optical response in metallic nanostructures," J. Phys. Condens. Matter **27**(18), 183204 (2015).
12. J. M. McMahon, S. K. Gray, and G. C. Schatz, "Nonlocal optical response of metal nanostructures with arbitrary shape," Phys. Rev. Lett. **103**(9), 097403 (2009).
13. J. M. McMahon, S. K. Gray, and G. C. Schatz, "Calculating nonlocal optical properties of structures with arbitrary shape," Phys. Rev. B **82**(3), 035423 (2010).
14. J. M. McMahon, S. K. Gray, and G. C. Schatz, "Optical properties of nanowire dimers with a spatially nonlocal dielectric function," Nano Lett. **10**(9), 3473–3481 (2010).
15. G. Toscano, M. Wubs, and S. Xiao, *et al.*, "Plasmonic nanostructures: local versus nonlocal response," Proc. SPIE **7757**, 77571T (2010).
16. G. Toscano, S. Raza, and A.-P. Jauho, *et al.*, "Modified field enhancement and extinction by plasmonic nanowire dimers due to nonlocal response," Opt. Express **20**(4), 4176–4188 (2012).
17. L. Stella, P. Zhang, and F. García-Vidal, *et al.*, "Performance of nonlocal optics when applied to plasmonic nanostructures," J. Phys. Chem. C **117**(17), 8941–8949 (2013).

Optics EXPRESS

18. R. Esteban, A. G. Borisov, and P. Nordlander, *et al.*, "Bridging quantum and classical plasmonics with a quantum-corrected model," Nat. Commun. **3**(1), 825–829 (2012).
19. L. Wu, H. Duan, and P. Bai, *et al.*, "Fowler–nordheim tunneling induced charge transfer plasmons between nearly touching nanoparticles," ACS Nano **7**(1), 707–716 (2013).
20. W. Zhu, R. Esteban, and A. G. Borisov, *et al.*, "Quantum mechanical effects in plasmonic structures with subnanometre gaps," Nat. Commun. **7**(1), 11495 (2016).
21. D. Xu, X. Xiong, and L. Wu, *et al.*, "Quantum plasmonics: new opportunity in fundamental and applied photonics," Adv. Opt. Photonics **10**(4), 703–756 (2018).
22. P. Zhang, "Scaling for quantum tunneling current in nano-and subnano-scale plasmonic junctions," Sci. Rep. **5**(1), 9826 (2015).
23. S. Banerjee and P. Zhang, "A generalized self-consistent model for quantum tunneling current in dissimilar metal-insulator-metal junction," AIP Adv. **9**(8), 085302 (2019).